



Synthesis and characterisation of activated carbon supported catalysts: photocatalytic degradation of olive wastewater solutions using these catalysts

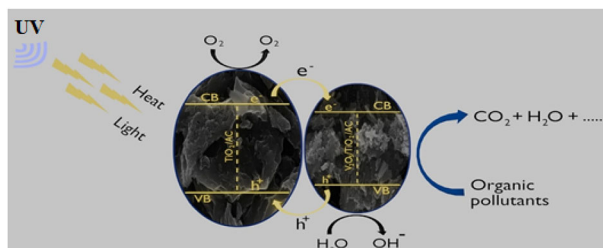
Huseyn Osman¹ · Selman İlateriş Yılmaz² · Mehmet Uğurlu¹ · Ali İmran Vaizoğullar³ · Abdul Jabbar Chaudhary⁴

Received: 12 August 2024 / Accepted: 26 May 2025
© The Author(s) 2025

Abstract

The aim of this study is to synthesize and characterize four different types of activated carbon supported catalysts and evaluate their effectiveness in the photocatalytic degradation of olive mill wastewater (OMW) generated during the olive oil production process. The four photocatalysts synthesized by using the sol-gel method were: TiO_2/AC , $\text{V}_2\text{O}_5/\text{TiO}_2/\text{AC}$, $\text{WO}_3/\text{TiO}_2/\text{AC}$ and $\text{V}_2\text{O}_5/\text{WO}_3/\text{TiO}_2/\text{AC}$. The photocatalysts were characterised by using TEM, SEM, XRD, FTIR analytical techniques and BET analyses. The degradation performance of these catalysts was evaluated by investigating the removal of pollutants such as color, phenol, lignin and COD from OMW. In addition, the effects on photocatalytic degradation were investigated in detail by considering the catalyst type, catalyst amount, suspension pH and contact time. From the experimental results, $\text{V}_2\text{O}_5/\text{TiO}_2/\text{AC}$ catalyst showed superior performance compared to the remaining catalysts. In order to increase the oxidation effect, ozone (O_3) and hydrogen peroxide (H_2O_2) were used as supporting oxidising agents either together or separately in some experiments. When ozone and UV were used together, the highest removal rates for color, phenol, lignin and COD were 87%, 91%, 60% and 70%, respectively, and when the catalyst and H_2O_2 were used together, the highest removal rates were 24%, 55%, 35% and 42%, respectively, for color, phenol, lignin and COD. When the catalyst, UV/ O_3 and H_2O_2 were used together, the removal rates for color, phenol, lignin and COD were 95%, 90%, 60% and 58%, respectively, after 6 hours. Under optimum conditions, photocatalytic degradation of various pollutants in the presence of supporting oxidants such as O_3 and H_2O_2 reached almost 80–95%. In conclusion, the findings of this research address a major environmental concern in the treatment of OMW by presenting an innovative catalytic method for the effective degradation of OMW wastewater.

Graphical Abstract



✉ Mehmet Uğurlu
mehmetu@mu.edu.tr

¹ Department of Chemistry, Faculty of Science. Muğla Sıtkı Kocman University, 48000 Muğla, Turkey

² Vocational School of Technical Sciences. Biomedical Technology Program. Istanbul University-Cerrahpasa, 34500 Istanbul, Turkey

³ Vocational School of Healthcare. Med Lab Program. Muğla Sıtkı Kocman University, 48000 Muğla, Turkey

⁴ College of Health, Medicine and Life Sciences. Department of Life Sciences. Division of Environmental Sciences. Brunel University London, London UB8 3PH, UK

Keywords Photocatalytic · Activated carbon · TiO₂ · WO₃ · V₂O₅ and Olive black water

Highlights

- TiO₂/AC, V₂O₅/TiO₂/AC, WO₃/TiO₂/AC and V₂O₅/WO₃/TiO₂/AC catalysts were synthesized by sol-gel method and the efficiency of these four different catalysts was investigated by photocatalytic treatment method for the removal of organic pollutants from olive oil wastewater (OMW) samples.
- The removal of various pollutants such as color, phenol, lignin and chemical oxygen demand (COD) was examined in detail under the effects of different experimental parameters.
- The V₂O₅/TiO₂/AC catalyst removed the determined pollutants at the highest rates.
- By using oxidants such as ozone (O₃) and hydrogen peroxide (H₂O₂), effective degradation of pollutants and increased removal rates have been observed.

1 Introduction

Considering the potential negative impacts of polyphenolic compounds, especially those found in OMW, on both economic values and treatment processes, they need to be removed from OMW. Various methods have been used, including liquid-liquid or liquid-solid extraction [1, 2], electrochemical oxidation [3, 4], chemical coagulation [5], filtration with membrane processes [6], ion exchange [7], extraction [8], biological treatment methods [9], catalytic processes [10, 11], evaporation and subsequent distillation [12] and adsorption [13–15]. Although these methods offer advantages, they also have several disadvantages that limit their widespread application [16]. All of these methods mainly consist of transferring the polluting components from the liquid phase to the solid phase or to another medium. In addition, these disadvantages include operating costs, accumulation of toxic by-products in the environment, high chemical consumption, complex operating processes and low efficiency are important issues which need to be addressed. In short, the treatment of olive wastewater is a very challenging process due to the presence of large number of different pollutants. The treatment methods briefly mentioned above may not be sufficient to reduce the concentration of harmful organic substances such as phenolic compounds in OMW to a sufficient level. Due to the special structure of OMW, new and more effective treatment technologies are needed.

In recent years, numerous studies have been conducted emphasizing that in addition to the strong adsorption properties of activated carbon, it can be used in catalytic reactions when loaded with semiconductor materials (as support material or catalyst carrier) [17]. However, among these substances, the most widely used substance is TiO₂ due to its cost and its lack of damage to biological systems [18]. The catalytic activity of TiO₂ can also be increased by loading on the activated carbon surface [19, 20].

Photodegradation of textile waste streams using TiO₂ semiconductor catalyst [21], removal of hydroxyphenol by TiO₂ film-coated solar photocatalytic reactor [22] and the removal of active pharmaceuticals called metoroprole by titanium-coated magnetic activated carbon (TiFeC) [23] have been reported in the literature.

Most of the studies reported in the literature use model solutions to investigate the effects of activated carbon supported catalysts on the degradation of various types of pollutants. However, a limited number of studies deal with the removal of organic pollutants from real industrial wastewater. There is a need to develop and optimize a photocatalytic degradation process using real industrial wastewater effluents. One of the most important and problematic real wastewater effluents is produced by the olive oil industry. It is reported that most of the existing treatment processes are not effective in the removal of different pollutants from olive mill wastewater due to toxicity and high concentration of organic compounds [24].

Although TiO₂/AC catalytic materials have been used for the treatment of different types of wastewater streams, however, their main aim was to reduce catalytic excitation and achieve higher removal rates. In the present study, the production of a catalytically active TiO₂/AC material by loading TiO₂ onto the activated carbon surface constituted the first stage of the study. Then, V₂O₅/TiO₂/AC, W₂O₅/TiO₂/AC and V₂O₅/WO₃/TiO₂/AC catalysts with high photocatalytic activity were synthesized by loading V₂O₅ and WO₃ to this material. Using these obtained materials, color, phenol, lignin and COD removal rates from olive wastewater (OMW) were investigated by photocatalytic oxidation process. Reaction time, catalyst type, amount (solid/liquid ratio), concentration and initial pH values were examined for process optimization. Photocatalytic degradation process was optimized by investigating the effects of various parameters.

Table 1 Physico-chemical characteristics of olive mill wastewaters sample

Parameters	Value
Colour	black
pH	5–6.6
COD (mg/L)	6.12×10^5
BOD (mg/L)	55.4
Polyphenol (mg/L)	8.0
Lignin (mg/L)	25.5
Density (25 °C) (g/L)	0.96
Conductivity ($\mu\text{S}/\text{cm}$)	7065

2 Materials and method

2.1 Chemicals

The chemicals used in all experimental studies and the sources from which they were supplied are briefly given below:

Activated carbon, Ammonium para tungstate $[(\text{NH}_4)_{10}\text{H}_2(\text{W}_2\text{O}_7)_6, 98\%]$ and Acetone ($\text{CH}_3\text{COCH}_3, 99\%$) were purchased from Sigma Aldrich. Titanium tetraisopropoxide $(\text{Ti}(\text{OCH}(\text{CH}_3)_2)_4, 98\%)$, Ammonium Monovanadate $(\text{NH}_4\text{VO}_3, 99\%)$, Hydrogen peroxide ($\text{H}_2\text{O}_2, 35\%$), pure ethanol ($\text{CH}_3\text{CH}_2\text{OH}$), Carbonate/tartrate reagent, Na_2CO_3 (sodium carbonate), sodium tartrate ($\text{Na}_2\text{C}_4\text{H}_2\text{O}_4, 99.5\%$), H_2SO_4 (95–97%), HgSO_4 (99%), Ag_2SO_4 (99%), $\text{K}_2\text{Cr}_2\text{O}_7$ (99.5%) and NaOH (97%) were obtained from Merck. HCl for pH adjustments was obtained from Riedel de Haen. Wastewater samples were taken from the local olive oil production facility which is the production period from Muğla region and in the winter season in accordance with the procedure and taken into sterile containers with certain storage conditions. The samples were taken to the laboratory and stored at +5 °C. Olive black water sample was diluted in certain proportions and used in all experimental studies since it contains high concentration of organic compounds. The characteristics of olive mill wastewater used in this work are presented in Table 1.

2.2 Synthesis of catalysts

For the synthesis of catalysts to be used in preliminary experimental work, 120 g of Titanium Tetraisopropoxide was added to 120 mL of 99.8% (v/v) ethanol. While the solution was stirred, 100 g of granulated activated carbon (AC), 8 mL of distilled water and 0.8 mL of Acetone, as a stabilizer, were added. It was observed that TiO_2 was formed as a result of 3 h of stirring and this resultant material was divided into four equal parts. The first part of the material was dried at 80 °C and allowed to cool to room

temperature, then calcined gradually. The product was labelled as TiO_2/AC . Then 2.19 g of ammonium monovanadate and 30 mL of ethanol were added into the second part and the resultant mixture turned into a gel by stirring for 2 hours. This material was dried at 80 °C and allowed to cool for calcination at room temperature. This material was labelled as $\text{V}_2\text{O}_5/\text{TiO}_2/\text{AC}$. The same procedure was used by adding 1.98 g of ammonium paratungstate and 30 mL of ethanol into the third part and the resultant product was labelled as $\text{WO}_3/\text{TiO}_2/\text{AC}$. Finally, 2.19 g of ammonium monovanadate, 1.98 g of ammonium paratungstate and 30 mL of ethanol and were added into the fourth part of the material and the mixture was stirred continuously for 2 h. After the mixture became gel, it was dried at 80 °C and allowed to cool to room temperature before calcination. This product was labelled as $\text{WO}_3/\text{V}_2\text{O}_5/\text{TiO}_2/\text{AC}$ respectively.

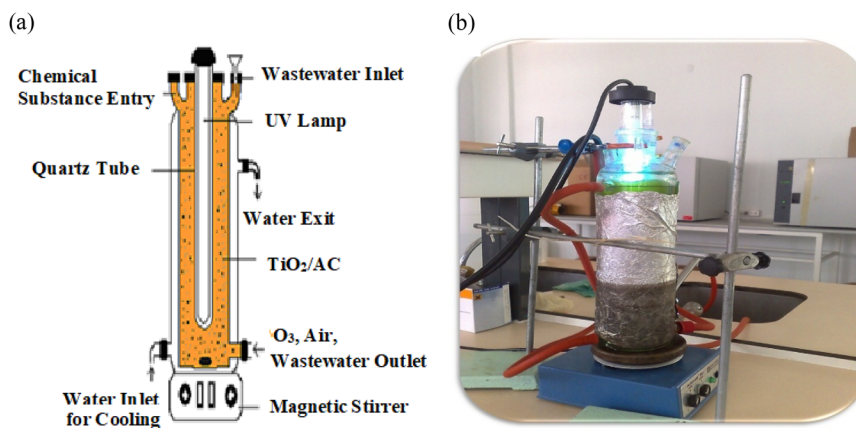
2.3 Calcination and experimental process

Granular activated carbon, which has adsorbed the catalytic material, was heated up to 300 °C under nitrogen gas flow in the ash furnace (PLF Series 110–130, Protherm). The temperature was kept constant at 300 °C for an hour and then the temperature was increased to 400 °C and kept constant at 400 °C for an hour. The calcined products were then allowed to cool naturally to room temperature. Photocatalytic experiments, by considering the studies in the literature, were carried out in UV reactor equipped with cooling feature, magnetic stirrer and UV lamp. The schema of the used reactor is shown in Fig. 1. Experiments were conducted to investigate the effects of various parameters such as reaction time, catalyst type, amount (as solid/liquid ratio), concentration and initial pH values.

2.4 The devices

The devices used and their purposes are briefly given below. WiseStir MSH 20 A model heated magnetic stirrer for mixing processes, Binder shear oven for drying processes, Nüve brand MF 140 model 6000Watt power muffle furnace for calcination processes, Specially manufactured reactor for photocatalytic oxidation experiments, Shimadzu brand UV 1601 model spectrophotometer for spectrophotometric measurements (in peak scanning), Dr. Hach Lange 2800 model spectrophotometer for COD measurements. Lange Dr 200 model thermostatic heater, WTW pH330i model digital pH meter for pH measurements, Jeol Jem 2100 model TEM device for TEM analyses, Jeol Jem 7600 F model SEM device for SEM analyses, Bruker 08 Advance model X-ray diffractometer for XRD analyses, BET analyses. Micrometrics Gemini 2380 model BET measuring device was used.

Fig. 1 Schematic view (a) and real view (b) of the experimental setup used in photocatalytic experiments



2.5 Analysis of wastewater

2.5.1 Determination of color

The percentage removal of color was investigated by taking wastewater samples at different time intervals during the oxidation process. These samples were centrifuged and the liquid phase obtained was used to monitor the changes in the absorbance in UV/visible region by using the spectrophotometric method. Based on the peak value observed at 400 nm wavelength (λ_{\max} value = 400 nm), the changes in absorbance intensity according to the initial conditions were followed and the percentage removal was calculated according to the equation:

$$\text{Color removal(\%)} = \frac{A_{\lambda}^0 - A_{\lambda}}{A_{\lambda}^0} 100 \quad (1)$$

Here, A_{λ}^0 refers to the initial absorbance and A_{λ} refers to the absorbance after the oxidation process.

2.5.2 Determination of lignin concentrations

By adding 0.2 mL of folin phenol and 2 mL of carbonate-tartrate reagents to a 10 mL wastewater sample, the mixture was allowed to stand for 30 minutes for complex formation, absorbance was measured at a wavelength of 700 nm. With the help of the calibration curve, the lignin concentrations were determined and the results were determined as the amount of substance that folinphenol reagent reduces [25].

2.5.3 Determination of COD amount

1.25 mL wastewater sample; 0.75 mL of digestion solution (potassium dichromate, mercury sulphate, sulfuric acid, water) and 1.75 mL of sulfate reagent (concentrated sulfuric acid, silver sulphate) is added to the thermostat heater, after

120 minutes at 148 °C, the COD was determined colorimetrically using a UV-spectrophotometer at 600 nm [25].

3 Discussion and conclusion

3.1 Characterisation of activated carbon supported catalytic materials

The characterisation of activated carbon supported (TiO_2/AC , $\text{V}_2\text{O}_5/\text{TiO}_2/\text{AC}$, $\text{WO}_3/\text{TiO}_2/\text{AC}$ and $\text{WO}_3/\text{V}_2\text{O}_5/\text{TiO}_2/\text{AC}$) catalytic materials and activated carbon was carried out using: scanning electron microscope the microstructure and morphology of the particles were analyzed using a scanning electron microscope (SEM, JEOL JSM-7600F). Transmission electron microscopy (TEM) images were acquired with a JEOL JEM-2100 (UHT) microscope. The crystalline structure was characterized by X-ray diffraction (XRD) with a Rigaku Dmax 350, utilizing copper $\text{K}\alpha$ radiation ($\lambda = 0.154056$ nm, JCPDS No. 21-1276). The FTIR spectra were recorded using an FTIR spectrometer operating in the range of 4000–400 cm^{-1} , with a spectral resolution of 4 cm^{-1} . Each spectrum was obtained by averaging 32 scans to enhance the signal-to-noise ratio. The samples were prepared in a KBr pellet form to ensure adequate transmission and minimize interference. The data were subsequently analyzed to identify characteristic absorption peaks, which correspond to specific molecular vibrations indicative of the material's composition and structure. The results obtained using these analytical techniques are discussed below.

3.2 SEM images

SEM images of nanocomposite materials before and after activation were obtained and can be seen in Fig. 2. In general, it has been observed that the pore size decreases depending on the surface area. It can be seen from the EDX

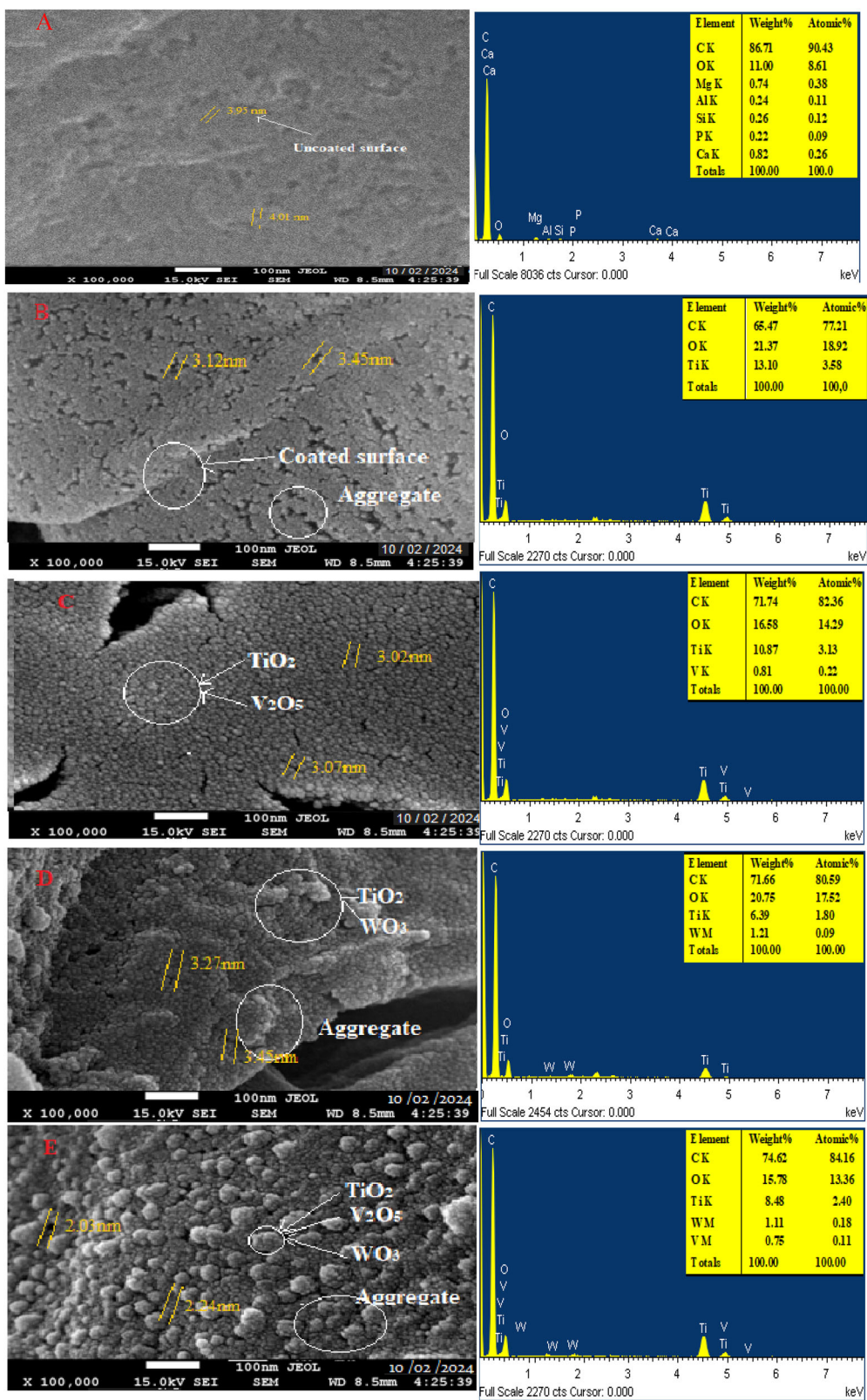
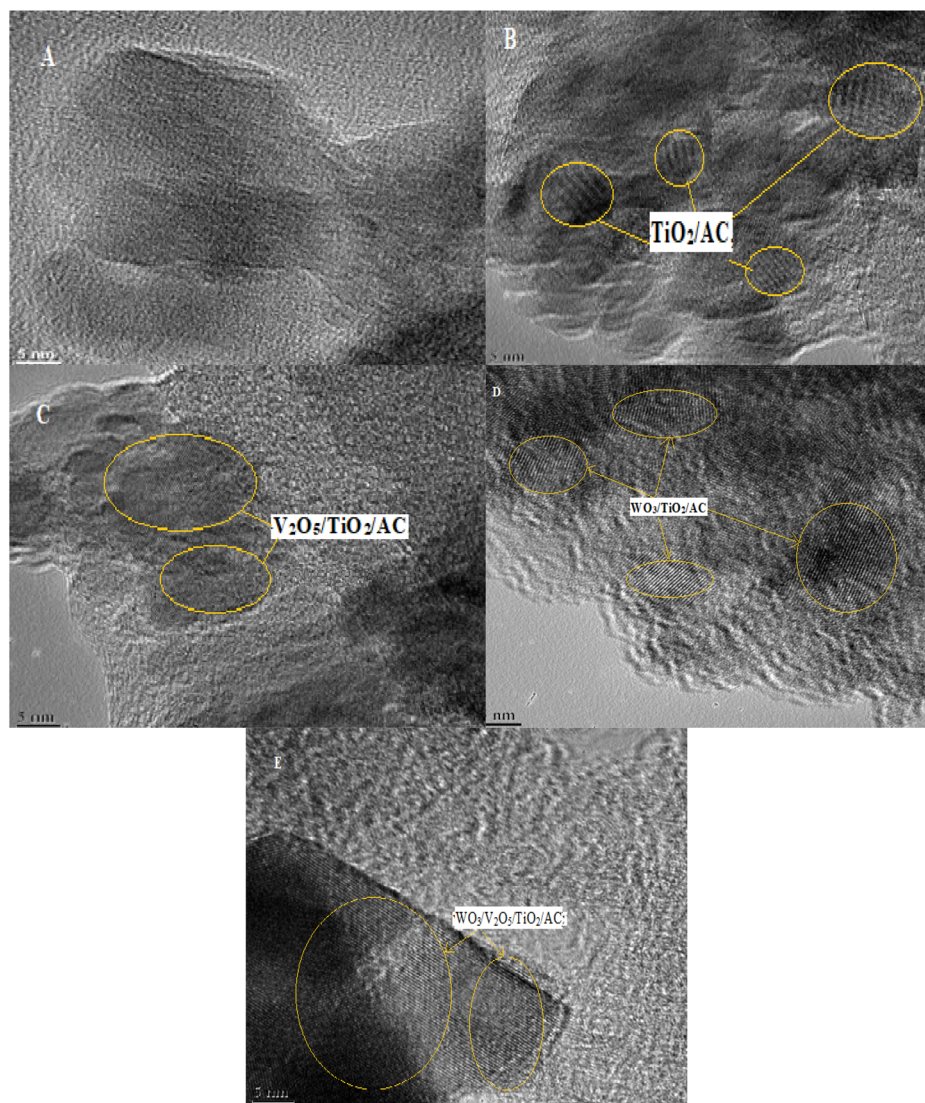


Fig. 2 SEM images of synthesized catalysts (A AC, B TiO₂/AC, C V₂O₅/TiO₂/AC, D WO₃/TiO₂/AC, E WO₃/V₂O₅/TiO₂/AC)

Fig. 3 TEM images of synthesized catalysts (A AC, B TiO_2/AC , C $\text{V}_2\text{O}_5/\text{TiO}_2/\text{AC}$, D $\text{WO}_3/\text{TiO}_2/\text{AC}$, E $\text{WO}_3/\text{V}_2\text{O}_5/\text{TiO}_2/\text{AC}$)



spectrum that AC consists mainly of 86% carbon and has a minimal amount of impurities.

SEM images of raw activated carbon and other synthesized catalytic materials were compared (Fig. 2). When Fig. 2A is examined, no significant change is observed on the AC surface. However, a certain change is observed when the surface is coated with TiO_2 . Here, it was observed that the sizes of stacked nanoparticle blocks decreased from approximately 4.0 nm to 3.12 nm and 3.45 nm with the addition of TiO_2 (Fig. 2B). On the other hand, a partial decrease in pore distribution was observed in the $\text{V}_2\text{O}_5/\text{TiO}_2/\text{AC}$ samples compared to the other two samples. Here, it was observed that the pore diameters were approximately 3.00 nm in size (Fig. 2C). This decrease is associated with the coating of the surface with components that have catalytic properties. In addition, it was observed that the pore distribution in $\text{WO}_3/\text{TiO}_2/\text{AC}$ samples generally occurred at values of 2.27 nm and 3.45 nm (Fig. 2D). The most obvious

change observed in the surface images was observed in $\text{WO}_3/\text{V}_2\text{O}_5/\text{TiO}_2/\text{AC}$ materials (Fig. 2E). Very distinct aggregates were seen here. EDX analyzes of all samples provide general information about the amounts and ratios of catalytic material retained on the surface.

3.3 TEM analysis

TEM images of the catalytic materials are given in Fig. 3. When the TEM images of all samples are examined, it can be seen that there is a clear appearance of catalysts on the surface of the AC samples. When all catalytic materials are examined, it is seen that homogeneous structures are distributed on the surfaces, but when the surfaces are examined in detail, there are differences on the surface. In general, the lace structure is seen more clearly in these examples. Additionally, in Fig. 3A, the effects of catalytic gasification and corrosion in AC samples are observed. In other samples, large scalloped particles of certain

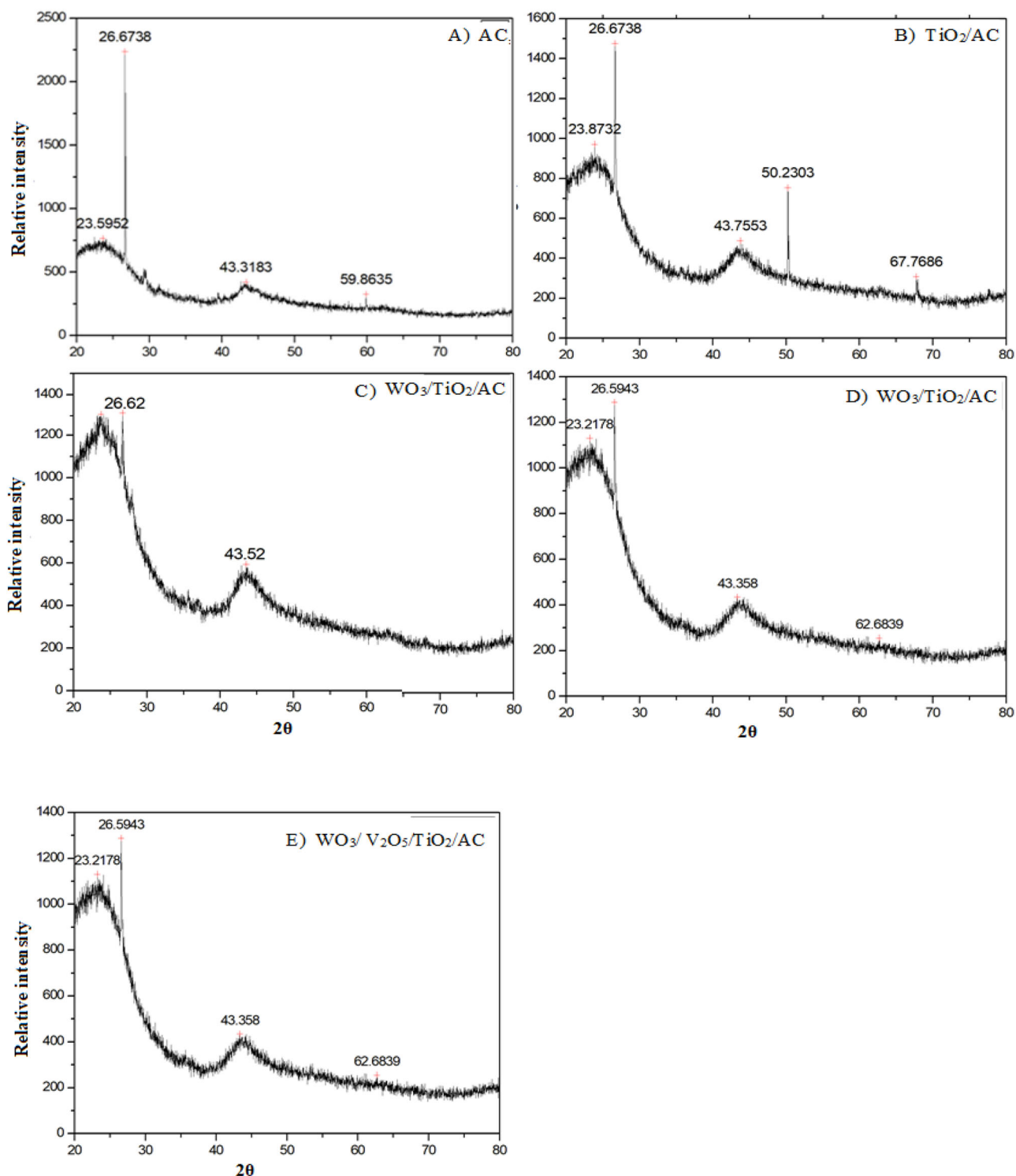


Fig. 4 XRD spectra of AC, all synthesized samples and combined samples (A-AC, B-TiO₂/AC, C-V₂O₅/TiO₂/AC, D-WO₃/TiO₂/AC, E-WO₃/V₂O₅/TiO₂/AC)

sizes and generally at the edges of the catalytic materials are observed. In addition, it is thought that particulate wear occurs in all catalytic particles, channelization may help to increase the pore size and thus transport the adsorbate to the interior of the particle.

3.4 XRD analysis

Figure 4A shows the XRD spectrum of AC. It shows that the highest intensity peak ($2\theta = 26.67$) belongs to hexagonal graphite. This shows that there is also a graphite structure in the

activated carbon structure and that this structure has a nanocrystalline character. The other peaks at $2\theta = 23.59^\circ$, 43.31° and 59.86° were evaluated as peaks belonging to the characteristic amorphous structure [26]. The values $2\theta = 23.8732^\circ$, 26.67° , 43.7553° , 50.2303° and 67.7686° seen in the XRD spectrum of TiO_2/AC define the rutile form of TiO_2 (Fig. 4B). Sharp and intense peaks indicate that TiO_2/AC has high crystallinity. The 2θ main peak values of monoclinic WO_3 and anatase TiO_2 are very close to each other [27]. As a result of the immobilization of WO_3 on the surface of the synthesized TiO_2/AC , a slight decrease in the peak intensity of TiO_2 was observed. This result shows that there is an effective dispersion of WO_3 on TiO_2 (Fig. 4C). Additionally, a slight shift to the left is observed in 2θ values (from 26.67 to 26.62). This shows that WO_3 is a single effective strain (uniform strain) within the TiO_2 mesh structure [28]. When the XRD spectrum of the $\text{V}_2\text{O}_5/\text{TiO}_2/\text{AC}$ composite material is examined (Fig. 4D), the value $2\theta = 23.2178$ appearing in the spectrum indicates the orthorhombic crystal structure of V_2O_5 . When the $\text{V}_2\text{O}_5/\text{TiO}_2/\text{AC}$ spectrum is examined (Fig. 4E), it shows that it is immobilized on TiO_2 , similar to $\text{WO}_3/\text{TiO}_2/\text{AC}$, and V_2O_5 causes a slight decrease in the peak intensity of TiO_2 . Additionally, as seen in the comparative XRD spectrum of AC and synthesized nanoparticles, characteristic peaks of AC, TiO_2 and V_2O_5 are observed (Fig. 4F). These results show that $\text{WO}_3/\text{TiO}_2/\text{AC}$ and $\text{V}_2\text{O}_5/\text{TiO}_2/\text{AC}$ composite particles were synthesized with high efficiency and provided an effective dispersion of catalytic components onto the AC surface. In addition, the XRD patterns provided in the study include the diffraction peaks of each component in the composite material. We understand that some peaks may appear less pronounced due to overlapping or lower crystallinity in certain phases, which can be challenging to distinguish clearly. However, upon careful analysis, characteristic peaks for activated carbon (AC), TiO_2 , WO_3 , and VO_x are identifiable within the noise level, supporting the presence of each component discussed in the paper. Furthermore, the observed diffraction peaks align with the known crystallographic planes of these materials, even though some may be more subtle due to phase interactions or composite structure. These overlaps can result from the synthesis method and the composite nature, leading to peak broadening or shifting. We believe that complementary characterization techniques, such as SEM-EDS or TEM, provide additional confirmation of the composition and distribution of phases, strengthening our findings beyond the XRD data alone.

3.5 BET analyzes

The BET surface areas of the AC used as the support solid for the catalytic material and the catalytic materials loaded on the AC were measured, and the results obtained are comparatively given in Table 2. In addition, the BET surface

area data of the best performing $\text{V}_2\text{O}_5/\text{TiO}_2/\text{AC}$ catalyst before and after photocatalytic use are shown comparatively.

When looking at the surface area between AC and TiO_2/AC , there is no big difference. This is due to the fact that TiO_2 immobilized on the activated carbon surface is adsorbed to some extent in the pores, not on the surface. However, after doping with V_2O_5 , the surface area decreased. This is due to the maximum dispersion of V_2O_5 on the TiO_2/AC surface. The slight decrease in the surface area after WO_3 addition is due to the aggregation of particles filling the silite pores. In general, there is no big difference between the surface areas except $\text{WO}_3/\text{V}_2\text{O}_5/\text{TiO}_2/\text{AC}$. The fact that the surface area is lower than before the reaction is associated with the effective adsorption of organic molecules on the catalyst surface.

3.6 FT-IR analyzes

FT-IR images of the synthesized catalysts are seen in Fig. 5. When AC and TiO_2 treated AC spectra were compared, -OH groups were observed at 3750 and 3630 cm^{-1} in both structures (Fig. 5). Considering the band intensities and widths, it can be seen that these groups do not undergo a significant change as a result of TiO_2 treatment. However, as in the -OH group, the shift to slightly higher frequencies can be interpreted as a change in the configuration of this group. In addition, in pure AC, the $\text{C}=\text{C}$ groups of the aromatic ring observed at 1580 cm^{-1} shift slightly and the peaks of titanium carboxylate vibrations appear at 1562 cm^{-1} , indicating that TiO_2 groups are placed in the gaps formed by the $\text{C}=\text{C}$ groups. In addition, the other peaks observed at 611 and 742 cm^{-1} belong to the Ti-O tension and are evidence of TiO_2 binding to the AC surface.

3.6.1 $\text{WO}_3/\text{TiO}_2/\text{AC}$

When the spectra of the product obtained after connecting WO_3 to the product obtained after connecting AC to TiO_2 were compared, the -OH group was observed at 3749 cm^{-1} (Fig. 5). In addition, it was observed that the CH_2 groups observed at 2924 cm^{-1} were almost not observed as a result of the addition of WO_3 due to its interaction with these groups. In addition, the titanium carboxylate peak observed as a result of TiO_2 addition disappeared with temperature, and a peak with less intensity appeared at 1580 cm^{-1} compared to pure AC. In addition, the new peak observed at 674 cm^{-1} belongs to the $\text{W}=\text{O}$ group and is an indication that WO_3 has been added to the structure.

3.6.2 $\text{V}_2\text{O}_5/\text{TiO}_2/\text{AC}$

When the spectrum of AC taken when V_2O_5 was added after TiO_2 was bound was examined, it was seen that the intensity of the OH group decreased and shifted to 3743 cm^{-1} .

Table 2 BET surface areas of synthesized catalysts

Surface area (m ² /g)	AC	TiO ₂ /AC	V ₂ O ₅ /TiO ₂ /AC	WO ₃ /TiO ₂ /AC	WO ₃ /V ₂ O ₅ /TiO ₂ /AC	V ₂ O ₅ /TiO ₂ /AC (Used)
	916,04	844,63	788,76	803,59	1004,62	392,36

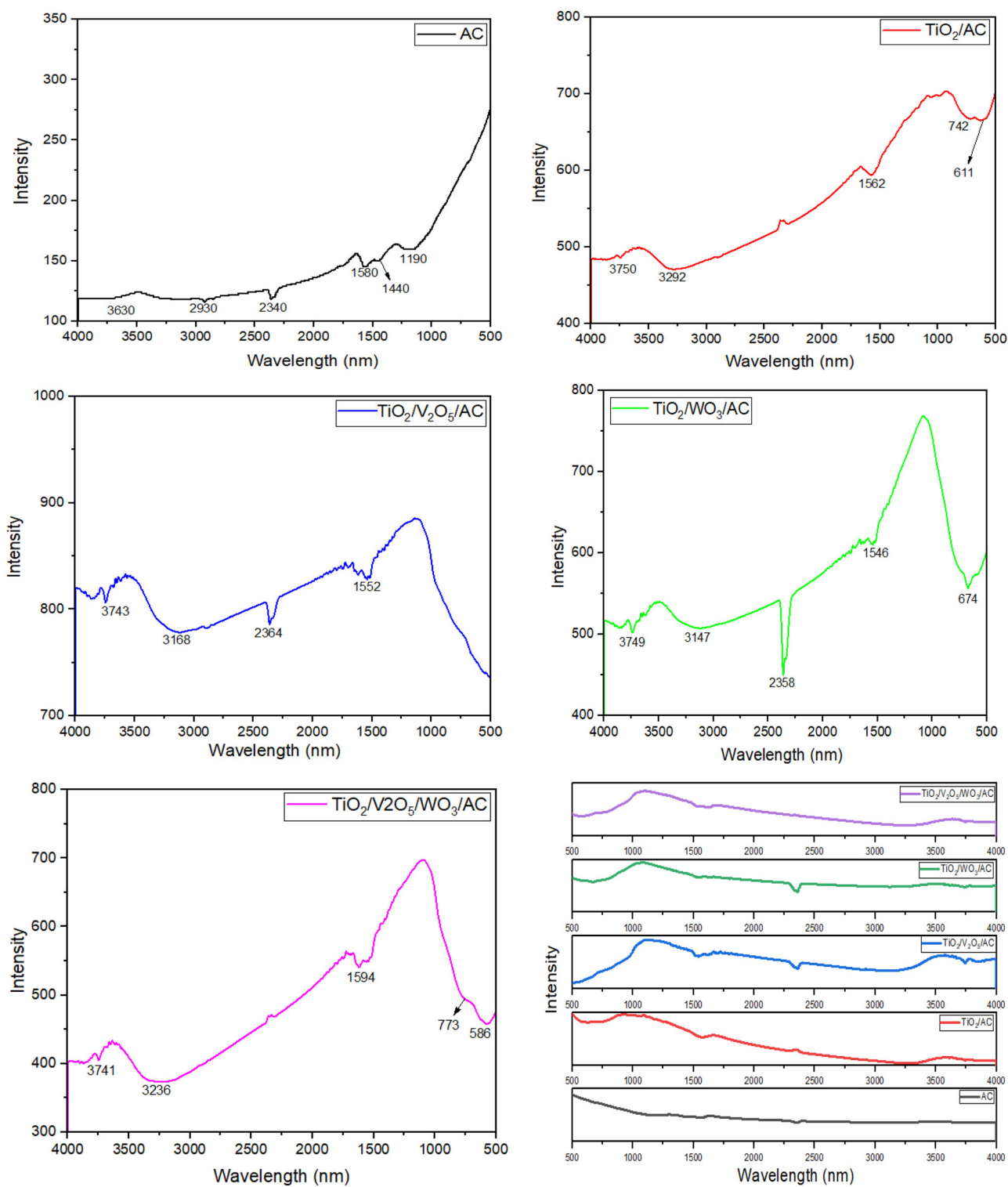
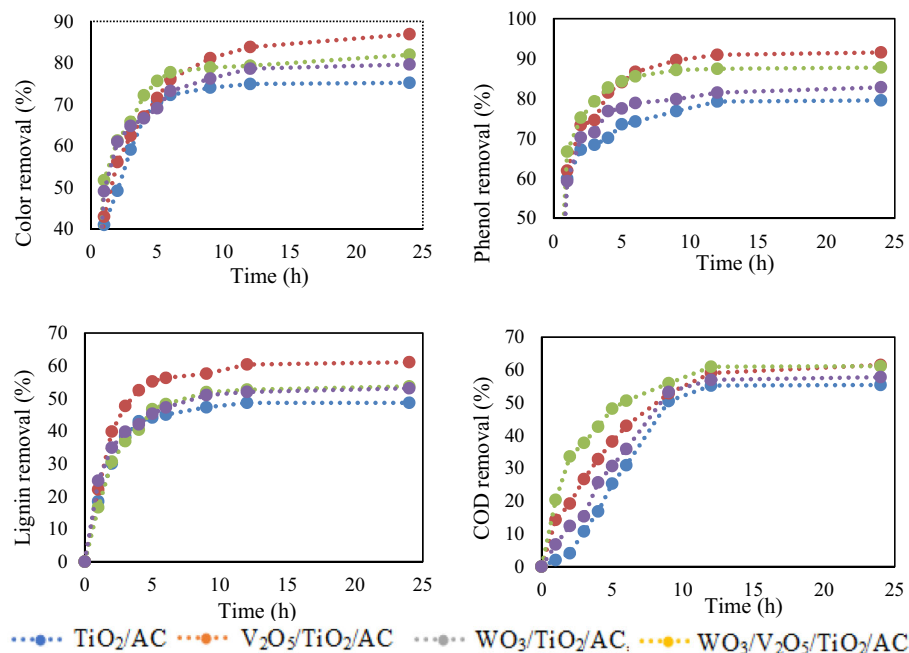


Fig. 5 FT-IR spectra of the synthesized catalysts compared to AC

Fig. 6 Removal rates for each catalyst (17 Watt UV, 1 g/L catalyst and natural pH)



Similar to WO_3 , CH_2 groups have disappeared. Similarly, with WO_3 binding, the titanium carboxylate groups observed at 1638 cm^{-1} disappeared and the $\text{C}=\text{C}$ stretching vibrations expected to be observed at 1575 cm^{-1} shifted to 1552 cm^{-1} with the V_2O_5 interaction. The $\text{C}-\text{O}$ peaks observed at 1190 cm^{-1} in pure AC were not clearly observed in both the $\text{WO}_3/\text{TiO}_2/\text{AC}$ and $\text{V}_2\text{O}_5/\text{TiO}_2/\text{AC}$ samples (Fig. 5). These results show that metal oxides are effectively immobilized on the AC surface.

3.7 Photocatalytic experiment results

Photochemical methods are basically based on the use of light radiation as an energy source. The source of photons can be natural sunlight or external UV light [29]. Color, phenol, lignin and COD removal rates were measured depending on time with four different catalysts (TiO_2/AC , $\text{TiO}_2/\text{WO}_3/\text{AC}$, $\text{TiO}_2/\text{V}_2\text{O}_5/\text{AC}$ and $\text{TiO}_2/\text{WO}_3/\text{V}_2\text{O}_5/\text{AC}$). All experiments were carried out using 17 Watt UV radiation lamp at a constant mixing speed. The degradation efficiency was examined by monitoring the changes in color, phenol, lignin and COD concentrations in olive mill water (OMW) samples taken at certain time intervals examined. Since OMW absorbs UV radiation, concentration was considered an important parameter. The effects of solid/liquid ratio, concentration and pH were evaluated with the catalyst showing the highest performance. Additionally, in order to increase the expected performance of the catalysts, the increase in OH^\bullet free radical formation and the extent to which the removal performances were affected by using H_2O_2 or O_3 were also

examined. To investigate the catalyst/UV effect, experiments were carried out using TiO_2/AC , $\text{WO}_3/\text{TiO}_2/\text{AC}$, $\text{V}_2\text{O}_5/\text{TiO}_2/\text{AC}$ and $\text{WO}_3/\text{V}_2\text{O}_5/\text{TiO}_2/\text{AC}$ catalysts. The results obtained are presented in Fig. 6.

In general, it is seen that the highest performance is achieved with $\text{V}_2\text{O}_5/\text{TiO}_2/\text{AC}$. Color, phenol, lignin and COD removal rates were achieved at 95%, 90%, 60% and 58%, respectively. Additionally, the second best color removal rate was achieved with $\text{WO}_3/\text{V}_2\text{O}_5/\text{TiO}_2/\text{AC}$. Adding supporting oxidising chemicals such as O_3 and H_2O_2 to increase the formation of superoxide, hydroxyl and ozonide radicals in the photocatalytic oxidation process is widely included in the literature [30–33]. To investigate the effect of O_3 and H_2O_2 in order to achieve higher removal and the expected performance in a short time, TiO_2/AC , $\text{WO}_3/\text{TiO}_2/\text{AC}$, $\text{V}_2\text{O}_5/\text{TiO}_2/\text{AC}$ and $\text{WO}_3/\text{V}_2\text{O}_5/\text{TiO}_2/\text{AC}$ catalysts were added to the reactor at 1.5°C . By providing L/min O_3 flow, time-dependent color, phenol, lignin and COD removal rates were investigated. The results obtained are graphed in Fig. 7.

The data presented in Fig. 7 show that when ozone was used together with UV, removal rates of 86.6%, 91.4%, 60.0% and 70% were achieved for color, phenol, lignin and COD, respectively, in a shorter time. The mechanism regarding the effect of O_3 current on the photocatalytic reaction is briefly schematized in Fig. 8.

It is seen that the removal performances increase significantly with the addition of O_3 to the photocatalytic reaction. Gomes et al. in their study on paraben removal from aqueous media using TiO_2 nanoparticles doped with Pt and Pd, found that the O_3 gas transferred into the

Fig. 7 Removal rates for each catalyst (17Watt UV, 1 g/L catalyst, 1.5 L/min O₃, and natural pH)

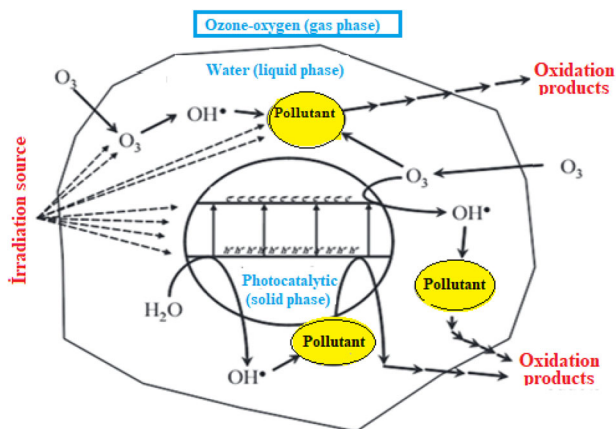
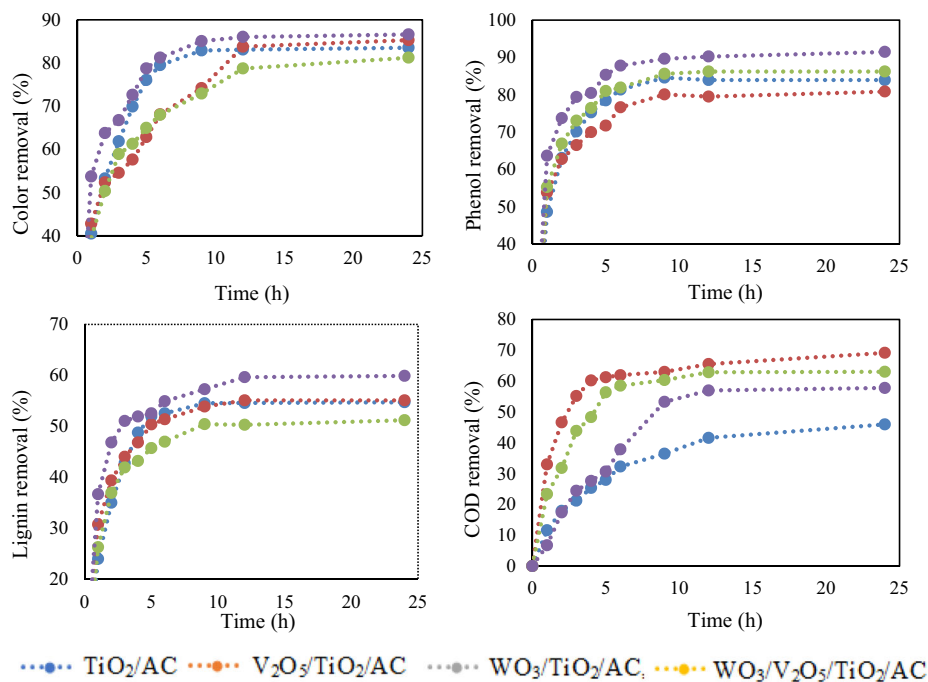
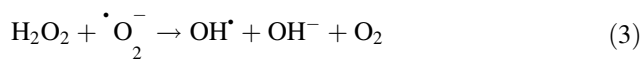


Fig. 8 Schematic view of the photocatalytic ozonation reaction performed with a heterogeneous catalyst [63]

reactor in the photocatalytic reaction increased photocatalytic degradation by forming ozonide and hydroxyl radicals [34]. They reported that this contributed significantly to its effect [35]. Although an increase in removal performance was observed due to the effect of O₃ current, no particular catalyst was clearly highlighted. Experiments were carried out under the same conditions with H₂O₂ (without the use of ozone), another oxidizing agent commonly used in advanced oxidation studies. By adding 1 mL/L H₂O₂ solution to the reactor with V₂O₅/TiO₂/AC catalysts, time-dependent changes in color, phenol, lignin and COD removal rates were investigated. The results obtained are graphed in Fig. 9.

When Fig. 9 is examined, for V₂O₅/TiO₂/AC, the highest color removal with the addition of H₂O₂ was obtained as 24% for phenol, 55%, for Lignin, 35% and for COD, 42%. Under UV irradiation, the O–O bonds of H₂O₂ are broken and OH• radicals are formed. On the other hand, it is thought that excess H₂O₂ in the environment reacts with the formed OH• radicals to form less reactive HO₂• radicals (Eqs. 2–5), therefore, the increase in the amount of peroxide in the photocatalytic degradation reaction may reduce the removal performance. This situation is expressed by the following reactions.



3.8 Solid/liquid ratio effect

In studies carried out using V₂O₅/TiO₂/AC catalyst and giving 1.5 L/min O₃ flow to the reactor; Color, phenol, lignin and COD removal rates were examined for 0.5, 1.0 and 1.5 g/L solid/liquid ratios. The results obtained are presented in Fig.10

When the effect of the solid/liquid ratio was examined, it was generally observed that the removal rates increased

Fig. 9 Removal rates for $V_2O_5/TiO_2/AC$ catalyst (17 Watt UV, 1 mL/L H_2O_2 , 1 g/L catalyst and natural pH)

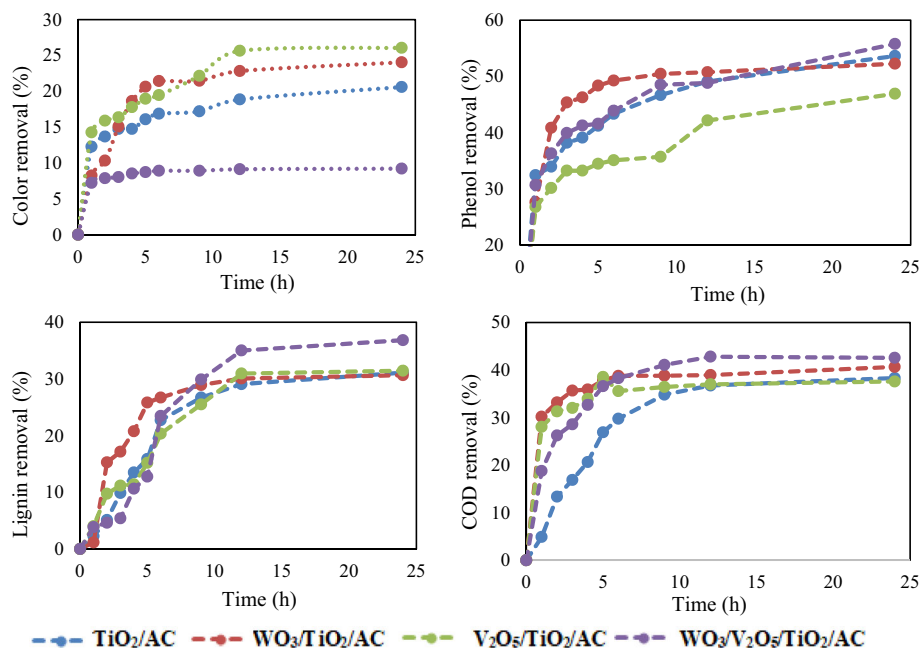
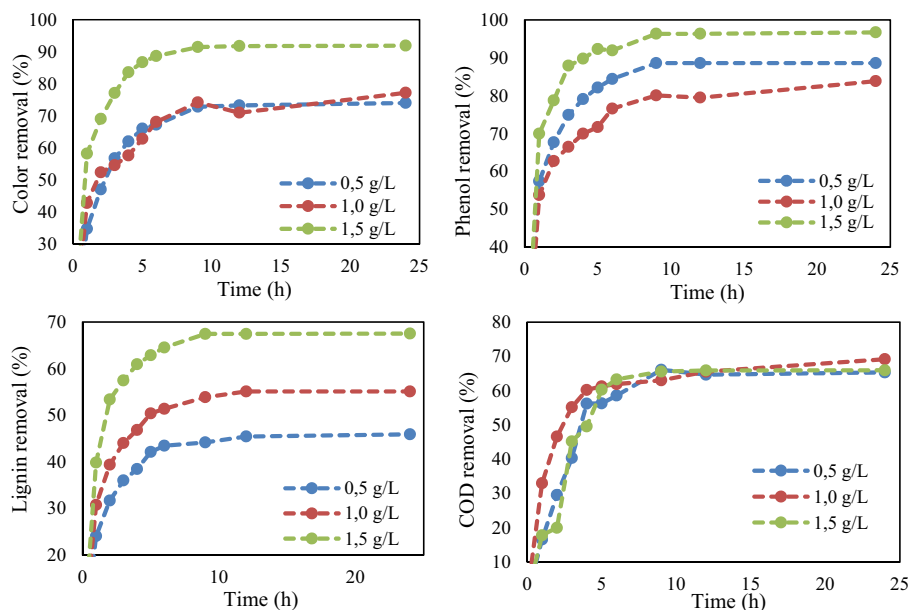


Fig. 10 Removal rates over time depending on the solid/liquid ratio (17 Watt UV, $V_2O_5/TiO_2/AC$, 1.5 L/min, O_3 and natural pH)



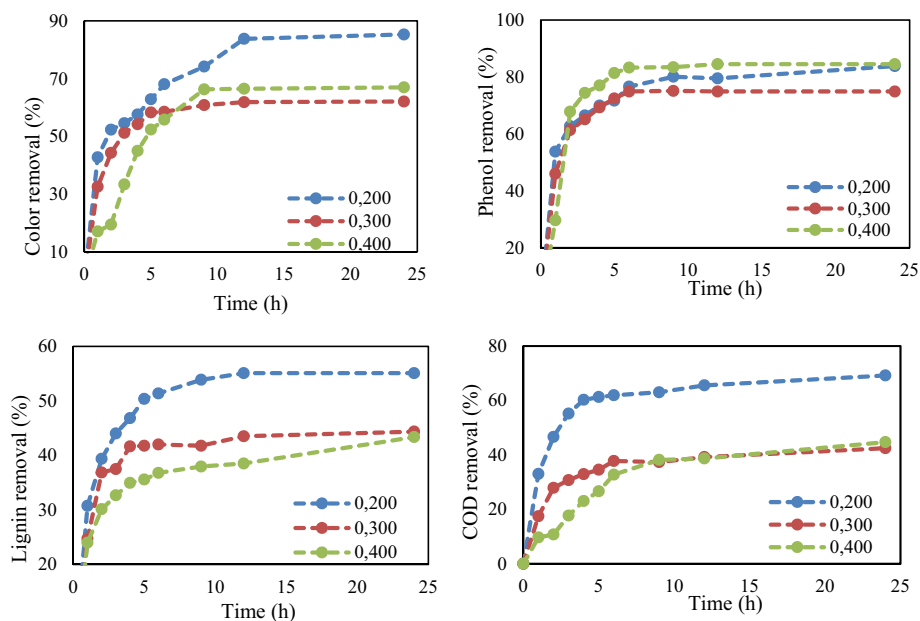
with the use of more catalyst. It was also observed in the reaction kinetics that the removal performance increased with increasing solid/liquid ratio. Lignin; It is a biopolymer synthesized and stored in plant cell walls together with cellulose and hemicellulose, which are responsible for providing mechanical strength and rigidity in the stems and stems of higher plants. It is reported that it is very difficult to degrade as it acts as a physical and chemical barrier against biodegradative systems [36]. Here, the fact that 68% lignin removal was achieved shows that a significant efficiency is achieved. When COD removals are evaluated, it is

seen that the solid/liquid effect is limited to the range of 65.3%- 69.2%. This can be explained by the decrease in the efficiency of the photocatalytic reaction as a result of the increase in the amount of particles blocking or absorbing UV rays.

3.9 Concentration effect

In studies carried out using 1.0 g/L $V_2O_5/TiO_2/AC$ catalyst and giving 1.5 L/min O_3 flow to the reactor; Color, phenol, lignin and COD removal rates were examined for 20%,

Fig. 11 Removal rates over time depending on concentration (17 Watt UV, 1 g/L $V_2O_5/TiO_2/AC$, 1.5 L/min O_3 and natural pH)



30% and 40% wastewater rates. The results obtained are presented in Fig. 11.

When color removals were examined depending on concentration, the highest rate was obtained for 20% wastewater (77.2%), while 62.1% and 66.9% color removals were achieved for wastewater diluted at 30% and 40%, respectively, after 24 hours. When phenol removal was evaluated, no significant difference was observed between 74.88% and 84.49%. When lignin and COD removals were examined, a decrease in removal rates was observed with increasing concentration. For 20% wastewater rate, lignin removal was obtained as 55.1%, and for 30% and 40% wastewater rates, 44.4% and 43.4% were obtained. A similar situation was observed for COD removal. In general, it appears that photocatalytic degradation is faster and more effective at low concentrations. This situation can be explained by the decrease in the photolytic effect due to the concentration-dependent increase in turbidity [37]. In addition, there are studies showing that the amount of photons participating in the reaction increases in parallel with the increase in the concentration of substances that absorb UV rays and that it does not have a negative effect as expected.

3.10 pH effect

In the study examining the pH effect, color, phenol, lignin and COD removal rates were examined according to the initial pH value. The natural pH value of the wastewater sample was observed as $pH = 5$, and the suspension pH was adjusted using HCl and NaOH solutions before the reaction. The results obtained are graphed in Fig. 12.

No exact correlation was observed between initial pH value and removal rates, and the highest color, phenol and lignin removal rates were observed for $pH=7$. When COD removal rates were examined, the highest removal rate was 80.8% for $pH = 3$. In the study conducted on the photocatalytic treatment of septic tank water with $WO_3/TiO_2/AC$, it was found that COD removal first decreased and then increased with increasing pH, and the increase observed for high pH was due to the conversion of OH^- ions into HO_3 radicals; It is reported that the high rate of degradation observed for low pH value may be due to the effect of positive holes on oxidation and the adsorption efficiency of the catalyst [38, 39]. In literature studies, it is well known that pH has a significant effect on TiO_2 photocatalysis systems [40, 41]. Additionally, a decrease in removals (except lignin) at low pH level (from 3 to 5) and a partial increase with increasing pH are observed in similar studies, with an increase in the degradation of organic substances, OH captured by photoproduced surface electron holes. It is reported that it results from the transformation of ions into hydroxyl radicals [42]. Moreover, although there is a partial decrease in the removal rate in the absence of OH^- ions, it is reported that positive vacancies instead of hydroxyl radicals may contribute to oxidation [43].

3.11 Catalyst, UV, O_3 and H_2O_2 effects

Experiments were also carried out to investigate the combined effects in the changes in color, phenol, lignin and COD removals that occurred in black water as a result of the adsorption of the catalytic material, the use of O_3 , H_2O_2 and UV effects alone or in double triples, and how each of these

Fig. 12 Removal rates over time depending on the initial pH value (17 Watt UV, 1 g/L $V_2O_5/TiO_2/AC$, 1.5 L/min O_3)

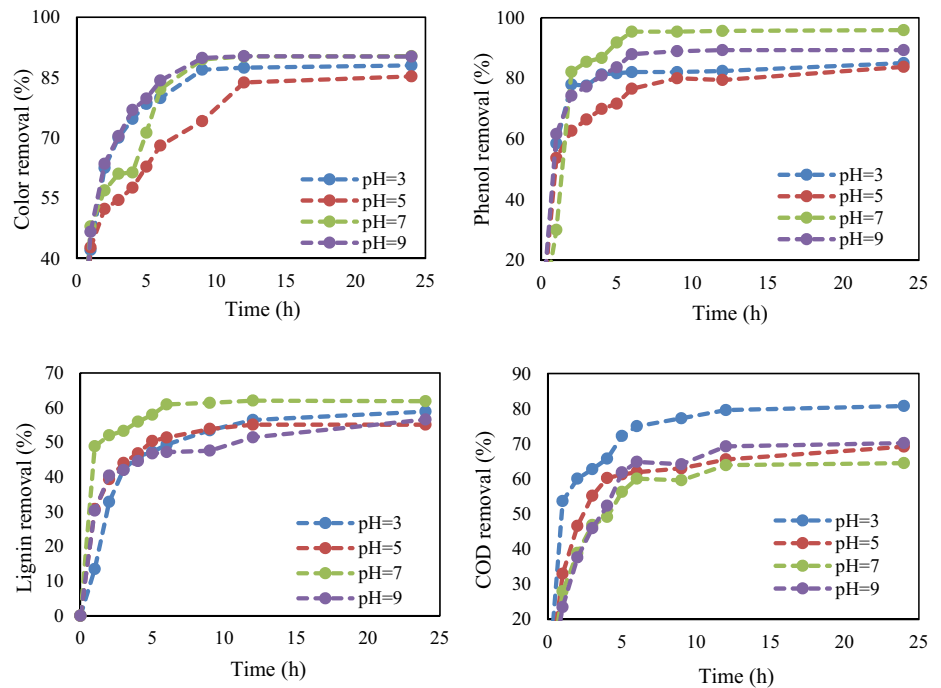
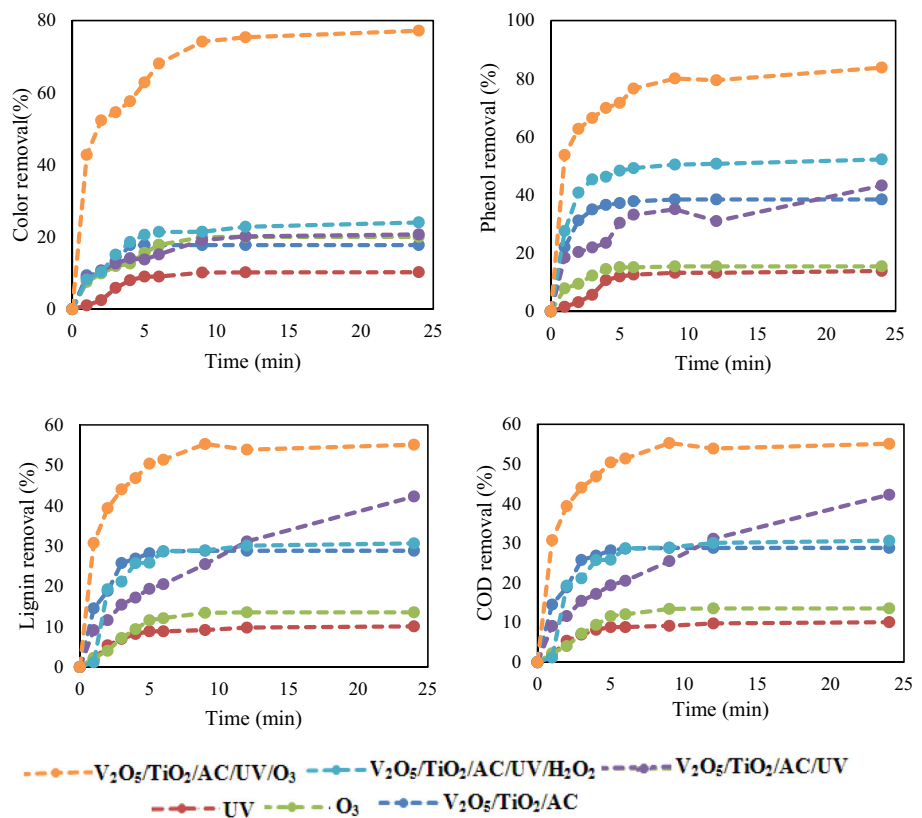


Fig. 13 Effects of catalyst, UV, H_2O_2 and O_3 on the photocatalytic oxidation mechanism (1.5 L/min O_3 , 1 mL/L H_2O_2 , 1 g/L catalyst and natural pH)

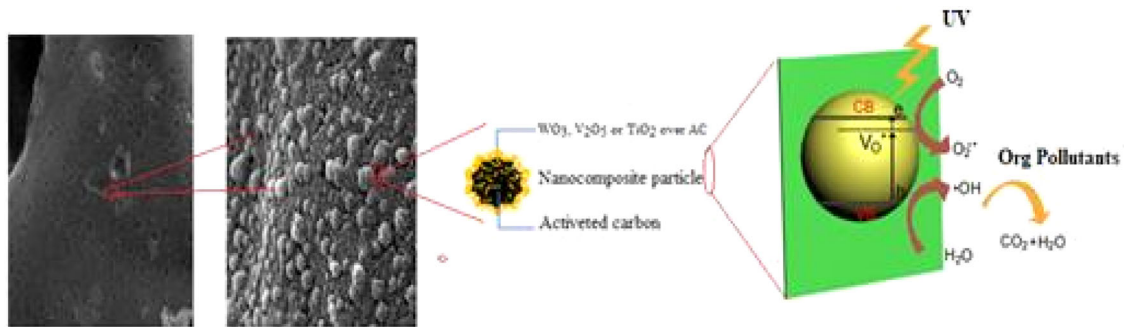


variables could contribute in the degradation process. The results obtained from the experimental study are presented in Fig. 13.

When a general comparison is made; The highest removal rates and fastest reaction kinetics without the use of ozone were obtained for $V_2O_5/TiO_2/AC$. When the

Table 3 Olive wastewater removal and degradation studies with different methods

Remediation techniques	Removal mechanism	Removal efficacy	Ref.
BiFeO ₃	Photocatalyst	Phenolic compounds- 82.9%, COD 98.0%	[49]
Fungi (<i>P. sajor caju</i> , <i>T. versicolor</i> and <i>P. chrysosporium</i>)	Photo-Fenton oxidation	Total phenolic content- (81–92%) COD-(53–76%)	[50]
H ₂ O ₂ /Cu (II)	Fenton-like system	Phenolic compounds- 62%	[51]
Zero-valent Fe/H ₂ O ₂	Fenton oxidation	COD- 92%	[52]
Aluminium electrodes	Electrocoagulation	COD-76%, Polyphenols-91% Colour-95%	[53]
H ₂ O ₂ /Fe ²⁺	Fenton's reagent	COD- 70%	[54]
UV/TiO ₂	Photocatalytic	Phenolic compounds-94%, COD- 22%, Color- 57%	[55]
Activated clay	Adsorption	Phenols-81%, organic matters-71%	[56]
TiO ₂ photocatalysis	Solar photocatalysis and solar photo-Fenton	Photo-Fenton method COD -85%, Phenol-90%	[57]
US/UV/TiO ₂	Photocatalytic	59% COD removal	[58]
Ozonation and UF	Advanced oxidation	UF followed by ozonation: BOD ₅ /COD = 0.55 20% COD and 93% TPh	[59]
Fenton's process and ozonation	Advanced oxidation proces	80% COD _s , 76.9% DOC and 72.6% color removal	[60]
Coagulation and Fenton's process	Treatment of OMW with integrated processes	45% COD removal 44% of biodegradability	[61]
Electrochemical oxidation	Electro / Fe ²⁺ / PS	71.2% COD 88% TPh	[62]
Activated Carbon Supported Catalysts	Photocatalytic	Color-%95, phenol-%90, lignin-%60, COD-%58	This study

**Fig. 14** Schematic representation of organic matter removal in the photocatalytic system

results were examined, the lowest efficiency was achieved in all pollutants when only UV was used. Afterwards, it was seen that maximum efficiency could be achieved by using V₂O₅/TiO₂/AC catalyst and H₂O₂ together, and finally using V₂O₅/TiO₂/AC/UV/O₃ together, respectively. In comparison to the color and phenol removals achieved over 80% by the effect of O₃ on the photocatalytic reaction, and the lignin and COD removals achieved at levels of 55% and 69%, respectively; The effect of H₂O₂ addition on the photocatalytic reaction was limited.

3.12 Comparison of the proposed method with other removal methods

The most commonly used wastewater treatment techniques entail physicochemical, chemical coagulation, precipitation, ion exchange (resin), and bioremediation (Table 3) methods. Most currently available methods (Table 3) have no data on the removal of lignin which is the main source of color and some methods reported that lignin removal is 60%. It is a well known fact that lignin biopolymer is resistant to both biological degradation and other methods.

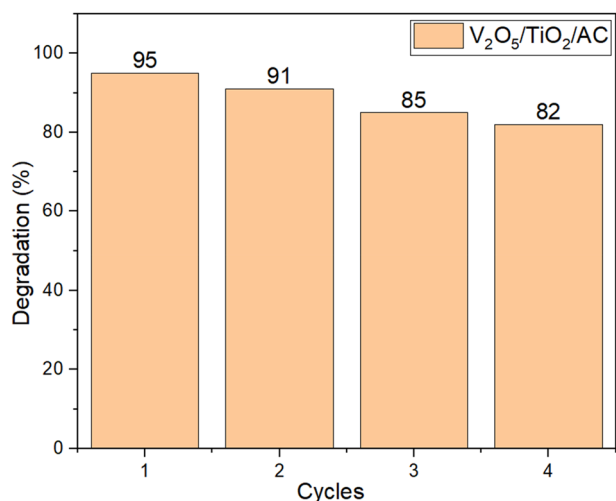


Fig. 15 Change in reusability of the catalyst

So, the proposed method provides a significant advantages over the currently available treatment methods. In addition, it was observed that color and phenol removal was also higher than the available methods.

3.13 Proposed photocatalytic mechanism

Instead of using granular activated carbon alone, a higher catalytic degradation rate can be obtained with semiconductor materials such as catalytic TiO_2 . Considering this situation, material with higher photocatalytic activity was obtained with $\text{TiO}_2/\text{V}_2\text{O}_5/\text{AC}$. Moreover, it is well known that hydroxyl radical ($\bullet\text{OH}$) can be used as strong oxidizing agent of organic compounds and plays an important role in oxidation. VO_2 valence and conduction bands are higher than TiO_2 . Therefore, V_2O_5 photochemically generated electrons are transferred to the conduction band of TiO_2 , and photogenerated holes in TiO_2 are transferred to the V_2O_5 valence band [44]. Photogenerated electrons and holes are thus highly segregated on the catalyst surface, enhancing catalytic activities. Moreover, the porous structures of AC will also increase the catalytic activity because more organic matter can be adsorbed. Considering that all decomposed catalysts are typical “nonactive” catalysts, water molecules on this “inactive” metal oxide surface (MOx) on the granular activated carbon surface readily dissociate to form physiologically potent oxidants [45]. A schematic representation of the possible mechanism related to the effect of OH, MOx ($\bullet\text{OH}$) ions, which can result in the complete oxidation of organic carbon to CO_2 , is given in Fig. 14.

It is thought that the V_2O_5 and TiO_2 on the granular activated carbon used can act as microcatalysis cells. In addition, another advantage of using granular particle is that the composite material can be easily recovered from the

solution after the photocatalytic reaction using a filter apparatus.

3.14 The active reactive oxygen species (ROS)

In the photocatalytic degradation study conducted with $\text{V}_2\text{O}_5/\text{TiO}_2/\text{AC}$, scavenger tests were performed to determine the active reactive oxygen species (ROS) responsible for the degradation process. These tests indicated that hydroxyl radicals ($\bullet\text{OH}$) played a more dominant role in the photocatalytic activity compared to other ROS. To identify the involvement of specific ROS, various scavengers were employed: isopropyl alcohol (IPA) was used as a scavenger for hydroxyl radicals, potassium iodide (KI) was used to quench holes (h^+), and superoxide p-benzoquinone (BQ) was utilized for superoxide radicals ($\text{O}_2\bullet$). The significant inhibition of degradation observed with IPA confirmed that hydroxyl radicals were the primary active species, while the effects of KI and BQ indicated a secondary but contributory role of holes and superoxide radicals. This understanding of ROS involvement provides insights into the mechanisms underlying the photocatalytic efficiency of the $\text{V}_2\text{O}_5/\text{TiO}_2/\text{AC}$ catalyst

3.14.1 Reusability of the $\text{V}_2\text{O}_5/\text{TiO}_2/\text{AC}$ catalyst

In the activated carbon supported catalyst system, a decrease in catalytic efficiency from 95% to 82% was observed after four cycles of reuse (Fig. 15). This observed decrease can be attributed to several interrelated factors affecting the surface properties and structural integrity of the catalyst. During successive cycles, organic and inorganic species are likely to accumulate on the catalyst surface, leading to surface fouling that clogs the active sites and disrupts interactions with target molecules, thereby impairing overall catalytic performance. Simultaneously, the high energy demands of the photocatalytic process may contribute to mechanical and chemical degradation of the catalyst, leading to erosion or deformation of the activated carbon support and decreased stability. In addition, the gradual loss or deactivation of active sites plays a significant role in this efficiency decrease. Active sites, such as metal atoms or functional groups critical for catalytic activity, may experience oxidative degradation or weakening of chemical bonds during repeated use, which may reduce their effectiveness.

3.15 Kinetic data

The degradation kinetics of the catalysts used were obtained by linearizing and evaluating the Preudo (pseudo) first order rate equation specified in (6).

$$\ln(C_t/C_o) = -kt \quad (6)$$

Table 4 Reaction rate constant (k) and R² values of photocatalytic oxidation

Parameters	Color		Phenol		Lignin		COD	
	K·10 ² (s ⁻¹)	R ²	K·10 ² (s ⁻¹)	R ²	K·10 ² (s ⁻¹)	R ²	K·10 ² (s ⁻¹)	R ²
Catalyst /UV effect								
TiO ₂ /AC	3.364	0.95	1.484	0.95	1.845	0.99	1.384	0.946
V ₂ O ₅ /TiO ₂ /AC	3.878	0.93	6.315	0.93	2.751	0.94	9.103	0.791
WO ₃ /TiO ₂ /AC	1.694	0.84	4.961	0.84	1.080	0.88	5.954	0.875
WO ₃ /V ₂ O ₅ /TiO ₂ /AC	2.462	0.93	4.129	0.93	2.244	0.97	3.533	0.842
Catalyst /UV/O ₃ effect								
TiO ₂ /AC	21.773	0.89	11.353	0.95	17.052	0.86	8.110	0.963
V ₂ O ₅ /TiO ₂ /AC	18.847	0.96	9.151	0.97	18.740	0.89	18.520	0.903
WO ₃ /TiO ₂ /AC	15.703	0.91	11.699	0.93	13.699	0.86	15.782	0.979
WO ₃ /V ₂ O ₅ /TiO ₂ /AC	19.761	0.87	11.621	0.89	17.227	0.80	14.681	0.905
Catalyst/UV/H ₂ O ₂ effect								
TiO ₂ /AC	3.281	0.80	10.326	0.82	3.556	1.00	5.982	0.99
V ₂ O ₅ /TiO ₂ /AC	3.964	0.95	11.908	0.83	6.298	0.92	8.284	0.84
WO ₃ /TiO ₂ /AC	3.427	0.92	9.002	0.70	3.734	0.98	7.593	0.83
WO ₃ /V ₂ O ₅ /TiO ₂ /AC	2.267	0.83	12.070	0.77	3.887	0.96	7.266	0.90
Catalyst/UV/H ₂ O ₂ /O ₃ effect								
TiO ₂ /AC	19.493	0.87	28.617	0.92	14.880	0.94	13.953	0.91
V ₂ O ₅ /TiO ₂ /AC	21.291	0.92	29.086	0.86	18.857	0.96	7.293	0.98
WO ₃ /TiO ₂ /AC	21.686	0.86	32.566	0.80	12.467	0.93	11.157	0.88
WO ₃ /V ₂ O ₅ /TiO ₂ /AC	19.238	0.85	25.644	0.76	13.133	0.88	8.295	0.93
S/L ratio effect								
0.5 g/L	17.787	0.91	21.449	0.91	9.795	0.86	15.075	0.99
1.0 g/L	18.847	0.96	23.943	0.96	18.740	0.85	18.520	0.90
1.5 g/L	33.767	0.93	47.464	0.93	22.226	0.91	18.463	0.96
Ozone effect								
0 L/min	3.491	0.87	6.315	0.93	2.751	0.94	6.859	0.85
0.75 L/min	5.924	0.91	13.727	0.96	6.888	0.94	13.611	0.82
1.50 L/min	18.847	0.96	23.943	0.92	18.740	0.85	18.520	0.90
2.25 L/min	44.799	0.98	49.289	0.94	19.058	0.85	25.846	0.97
Concentration effect								
%20	18.847	0.96	23.943	0.92	18.740	0.85	18.520	0.90
%30	16.184	0.89	20.434	0.85	12.639	0.85	7.194	0.83
%40	13.776	0.99	28.220	0.88	12.712	0.84	5.367	0.97
pH effect								
pH=3	25.654	0.91	25.802	0.69	13.595	0.92	23.598	0.97
pH=5	18.847	0.96	18.847	0.92	15.740	0.85	18.520	0.90
pH=7	22.751	0.94	46.316	0.92	15.755	0.89	14.064	0.94
pH=9	28.390	0.94	29.885	0.86	18.228	0.90	17.136	0.98
Catalyst/UV/H ₂ O ₂ effect								
AC	1,55	0,86	1,48	0,91	1,72	0,89	1,97	0,92
V ₂ O ₅ /TiO ₂ /AC	1.469	0.87	2.905	0.90	1.666	0.92	1.857	0.92
UV	1.823	0.95	2.534	0.96	2.237	0.97	2.435	0.98
O ₃	2.861	0.93	3.627	0.92	2.494	0.99	3.967	0.96
V ₂ O ₅ /TiO ₂ /AC/UV/ H ₂ O ₂	3.878	0.93	6.315	0.93	2.751	0.94	15.312	0.85
V ₂ O ₅ /TiO ₂ /AC/UV/O ₃	3.964	0.95	11.908	0.83	6.298	0.92	8.284	0.84
V ₂ O ₅ /TiO ₂ /AC/UV/ H ₂ O ₂ /O ₃	18.847	0.96	9.151	0.97	18.740	0.89	18.520	0.90

Here, C_0 refers to the initial concentration (mg/L), C_t refers to the concentration at time t (mg/L), time t and k refers to the pseudo 1st order rate constant, as proven by regression analysis ($R^2 > 0.70$). The higher rate constant obtained by using the catalyst can be explained by the combined effects of the adsorption of the organic molecule on the catalyst surface and the oxidation that occurs by the direct attack of the hydroxyl radicals produced on the positive voids formed afterwards [46]. Reaction rate constants for electrocatalytic, photocatalytic oxidation processes are given in Table 4, respectively.

When Table 4 is examined, it is seen that a kinetic increase is obtained in all experimental conditions when $V_2O_5/TiO_2/AC$ and UV are used together. It is observed that the K value increases more in all species when H_2O_2 is added. In addition, it is observed that a greater increase is provided when $V_2O_5/TiO_2/AC/UV/O_3$ is used together. When $V_2O_5/TiO_2/AC/UV/H_2O_2/O_3$ systems are used together, it is seen that the efficiency is kinetically higher. It is expected that catalytic decomposition may be higher in the presence of oxidizing agents in the environment. In addition, it can be concluded that the efficiency may be better at high pH. As it is known, pH changes are considered an important step for photocatalytic oxidation to occur since they can affect the adsorption of substrate molecules to the catalyst surfaces. Secondly, reactions occur between the OH ion and the positive hole on the surface of the semiconductor material. The formation of OH ions in alkaline environment will increase the formation of radical ions. It is also reported that in photocatalytic oxidation with heterogeneous catalysts, degradation can occur faster at alkaline pH than at acidic pH range [47]. In addition, the increase in efficiency at high pH can be explained by the weak adsorption of organic substrates to the catalyst, but they are attacked by OH. On the other hand, the partial decrease in efficiency at low pH can be associated with the reduced availability of the catalyst surface as a result of agglomeration of catalyst particles [48]. This situation may result in a decrease in the rate of heterogeneous photocatalytic oxidation at acidic pH.

3.16 Future perspective and sustainability of management

When the future perspective of the study is evaluated, due to the intense interest in photocatalysis processes, its widespread use in the removal of organic materials and its importance in sustainable chemistry have recently increased. While addressing environmental pollution, the effective use of photolytic radiation while preserving its environmentally friendly feature is seen as indispensable in research and material technologies. In addition, the use

of renewable energies to activate oxidation and reduction based chemical reactions via photocatalysis is an important technological approach that is applicable and sustainable to address environmental challenges. In the presented study, the use of photocatalysis systems, especially the removal of organic pollutants such as OMW, wastewater, residual paint and similar, is observed as a very promising approach to address environmental problems. The present study concerns with the use of photocatalytic material in a photochemical process resulting from the loading of a semiconductor onto a porous and high surface area material. In particular, this process shows that two simultaneous reactions occur: an initial oxidation reaction due to photoinduced positive holes and a subsequent reduction reaction whose formation is due to photoinduced negative electrons. This material exhibiting high potential as a photocatalyst holds promise for widespread use in waste management systems with a focus on environmental sustainability.

4 Conclusion

In the photocatalytic oxidation study seeking a solution to the pollution problem in olive oil wastewater samples, four new activated carbon-supported catalyst materials were synthesized and comprehensive characterization studies were conducted. In photocatalytic oxidation experiments, $V_2O_5/TiO_2/AC$ catalyst was observed to perform more effectively than other catalyst materials. In catalytic studies conducted with this material:

- Color, phenol, lignin and COD removal rates were obtained as 95%, 90%, 60% and 58%, respectively.
- In the oxidation process where ozone and UV light were used together, these rates increased to 87%, 91%, 60% and 70% in a shorter time.
- Where catalyst and H_2O_2 were used together, the percentage degradation were reduced to 24%, 55%, 35% and 42% in the system. This showed that no significant difference was observed between the catalysts when H_2O_2 or O_3 was added to the medium.

In addition, it was observed that the effect of pH on photocatalytic oxidation was limited and the increase in catalyst concentration and amount reduced turbidity and light transmittance and could limit the photocatalytic effect. As a result, it is seen that the photocatalytic method used in the treatment of olive oil wastewater is an effective and economically viable treatment technology. It is thought that the catalytic materials to be developed with TiO_2 as the main catalytic material can make significant contributions to wastewater treatment technologies.

Data availability

The experimental findings, results or content presented in the article have not been used in any other study or publication. Should any raw data files be needed in another format they are available from the corresponding author upon reasonable request. Source data are provided with this paper.

Acknowledgements This study was financially supported as a project (16/146) by Research Project Coordination Unit, Muğla Sıtkı Koçman University.

Author contributions The literature study and experiments of the article were done by Huseyn Osman and Selman İleriş Yılmaz. The characterization studies and evaluation of the material were carried out by Assoc. Prof. Dr. Ali İmran Vaizoğullar. The writing of the article considering the results obtained was done by Prof. Dr. Mehmet Uğurlu and the grammatical evaluation was done by Dr. Abdul Jabbar Chaudhary

Funding Open access funding provided by the Scientific and Technological Research Council of Türkiye (TÜBİTAK).

Compliance with ethical standards

Conflict of interest The authors declare no competing interests.

Ethics There is no ethical violation in our study.

Publisher's note Springer Nature remains neutral with regard to jurisdictional claims in published maps and institutional affiliations.

Open Access This article is licensed under a Creative Commons Attribution 4.0 International License, which permits use, sharing, adaptation, distribution and reproduction in any medium or format, as long as you give appropriate credit to the original author(s) and the source, provide a link to the Creative Commons licence, and indicate if changes were made. The images or other third party material in this article are included in the article's Creative Commons licence, unless indicated otherwise in a credit line to the material. If material is not included in the article's Creative Commons licence and your intended use is not permitted by statutory regulation or exceeds the permitted use, you will need to obtain permission directly from the copyright holder. To view a copy of this licence, visit <http://creativecommons.org/licenses/by/4.0/>.

References

- Al-Qodah Z, Al-Zoubi H, Hudaib B, Omar W, Soleimani M, Abu-Romman S, Frontistis Z (2022) Sustainable vs. conventional approach for olive oil wastewater management: a review of the state of the art. *Water* 14(11):1695
- Fernandes MJ, Gomes J, Carvalho P, Martins RC, Domingues E (2024) Removal and recovery of phenolic compounds from OMW by a cationic resin. *Chem Eng Sci* 291:119925
- Zhu Y, Nie J, Yang X, Guan X (2021) Degradation of tetrabromobisphenol A by ferrate (VI)-CaSO₃ process: kinetics, products, and impacts on following disinfection by-products formation. *J Hazard Mater* 412:125297
- Savić BG, Stanković DM, Živković SM, Ognjanović MR, Tasić GS, Mihajlović IJ, Brdarić TP (2020) Electrochemical oxidation of a complex mixture of phenolic compounds in the base media using PbO₂-GNRs anodes. *Appl Surf Sci* 529:147120
- Golbaz S, Jafari AJ, Rafiee M, Kalantary RR (2014) Separate and simultaneous removal of phenol, chromium, and cyanide from aqueous solution by coagulation/precipitation: Mechanisms and theory. *Chem Eng J* 253:251–257
- Sánchez-Arévalo CM, Jimeno-Jiménez Á, Carbonell-Alcaina C, Vincent-Vela MC, Álvarez-Blanco S (2021) Effect of the operating conditions on a nanofiltration process to separate low-molecular-weight phenolic compounds from the sugars present in olive mill wastewaters. *Process Saf Environ Prot* 148:428–436
- Ochando-Pulido JM, Vellido-Pérez JA, González-Hernández R, Martínez-Férez A (2020) Optimization and modeling of two-phase olive-oil washing wastewater integral treatment and phenolic compounds recovery by novel weak-base ion exchange resins. *Sep Purif Technol* 249:117084
- Sulaiman R, Adeyemi I, Abraham SR, Hasan SW, AlNashef IM (2019) Liquid-liquid extraction of chlorophenols from wastewater using hydrophobic ionic liquids. *J Mol Liq* 294:111680
- Mareai BM, Fayed M, Aly SA, Elbarki WI (2020) Performance comparison of phenol removal in pharmaceutical wastewater by activated sludge and extended aeration augmented with activated carbon. *Alex Eng J* 59(6):5187–5196
- Oladipo AA (2021) Rapid photocatalytic treatment of high-strength olive mill wastewater by sunlight and UV-induced CuCr₂O₄@ CaFe-LDO. *J Water Process Eng* 40:101932
- Oladipo AA (2021) CuCr₂O₄@ CaFe-LDO photocatalyst for remarkable removal of COD from high-strength olive mill wastewater. *J Colloid Interface Sci* 591:193–202
- Sklavos S, Gatidou G, Stasinakis AS, Haralambopoulos D (2015) Use of solar distillation for olive mill wastewater drying and recovery of polyphenolic compounds. *J Environ Manag* 162:46–52
- Al Bsoul A, Hailat M, Abdelhay A, Tawalbeh M, Al-Othman A, Al-Taani AA (2021) Efficient removal of phenol compounds from water environment using Ziziphus leaves adsorbent. *Sci Total Environ* 761:143229
- Şenel S, Kara A, Alsancak G, Denizli A (2006) Removal of phenol and chlorophenols from water with reusable dye-affinity hollow fibers. *J Hazard Mater* 138(2):317–324
- Osman B, Özer ET, Kara A, Yeşilova E, Beşirli N (2015) Properties of magnetic microbeads in removing bisphenol-A from aqueous phase. *J Porous Mater* 22:37–46
- Soukaina EA, Hajar EM, Mohamed D, Abdelmjid B, Brahim A, José ÍC, Najib T (2024) Enhancing the performance of alumina-pillared clay for phenol removal from water solutions and polyphenol removal from olive mill wastewater: Characterization, kinetics, adsorption performance, and mechanism. *J Water Process Eng* 63:105432
- Mahmoodi NM, Arami M, Limaee NY, Tabrizi NS (2005) Decolorization and aromatic ring degradation kinetics of Direct Red 80 by UV oxidation in the presence of hydrogen peroxide utilizing TiO₂ as a photocatalyst. *Chem Eng J* 112(1-3):191–196
- Iervolino G, Sannino D, Pepe G, Basilicata MG, Campiglia P, Vaiano V (2023) An effective way for the simultaneous valorization and treatment of olive mill wastewater by means of a photocatalytic process. *Chem Eng J* 468:143725
- Zhang SJ, Yu HQ, Zhao Y (2005) Kinetic modeling of the radiolytic degradation of Acid Orange 7 in aqueous solutions. *Water Res* 39(5):839–846
- Bekkouche S, Bouhelassa M, Salah NH, Meghlaoui FZ (2004) Study of adsorption of phenol on titanium oxide (TiO₂). *Desalination* 166:355–362

21. Rao NN, Chaturvedi V, Pumac GL (2012) Novel pebble bed photocatalytic reactor for solar treatment of textile wastewater. *Chem Eng J* 184:90–97
22. Martínez S, Morales-Mejía JC, Hernández PP, Santiago L, Almanza R (2014) Solar photocatalytic oxidation of Triclosan with TiO₂ immobilized on volcanic porous stones on a CPC pilot scale reactor. *Energy Procedia* 57:3014–3020
23. Rey A, Quinones DH, Álvarez PM, Beltrán FJ, Plucinski PK (2012) Simulated solar-light assisted photocatalytic ozonation of metoprolol over titania-coated magnetic activated carbon. *Appl Catal B: Environ* 111:246–253
24. Çifçi Dİ, Meriç (2015) Optimization of suspended photocatalytic treatment of two biologically treated textile effluents using TiO₂ and ZnO catalysts. *Global NEST Journal* 17(4):653–663
25. Uğurlu M, Kula İ (2007) Decolourization and removal of some organic compounds from olive mill wastewater by advanced oxidation processes and lime treatment. *Environ Sci Pollut Res* 14:319–325
26. Mirgorod Y, IEmelianov S, Fedosjuk V, Bolshanina S (2016) Influence of Size Effects on the Properties of Processed Iron Ore and Schungite Rock. *J Nano- Electron Phys* 8(2):2053–1
27. Yu SQ, Ling YH, Wang RG, Zhang J, Qin F, Zhang ZJ (2018) Constructing superhydrophobic WO₃@ TiO₂ nanoflake surface beyond amorphous alloy against electrochemical corrosion on iron steel. *Appl Surf Sci* 436:527–535
28. Rostami M, Mazaheri H, Hassani JA, Shokri A (2019) Using experimental design to optimize the photo-degradation of P-nitro toluene by nano-TiO₂ in synthetic wastewater. *Int J Eng* 32(8):1074–1081
29. Najafi A (2017) A novel synthesis method of hierarchical mesoporous MgO nanoflakes employing carbon nanoparticles as the hard templates for photocatalytic degradation. *Ceram Int* 43(7):5813–5818
30. Reddy PVL, Kim K (2015) A review of photochemical approaches for the treatment of a wide range of pesticides. *J Hazard Mater* 285:325–335
31. Touati A, Hammedi T, Najjar W, Ksibi Z, Sayadi S (2016) Photocatalytic degradation of textile wastewater in presence of hydrogen peroxide: Effect of cerium doping titania. *J Ind Eng Chem* 35:36–44
32. Shokri A, Nasernejad B (2024) Investigation of spent caustic effluent treatment by electro-peroxone process; cost evaluation and kinetic studies. *J Ind Eng Chem* 129:170–179
33. Shokri A, Karimi S (2022) Treatment of dinitrotoluene in an aqueous environment by electro-peroxodisulfate process using a central composite design. *Desalination Water Treat* 272:209–219
34. Mehrjouei M, Müller S, Möller D (2015) Decomposition kinetics of MTBE, ETBE and, TAEE in water and wastewater using catalytic and photocatalytic ozonation. *J Mol Catal A: Chem* 386:61–68
35. Gomes HT, Figueiredo JL, Faria JL (2007) Catalytic wet air oxidation of olive mill wastewater. *Environ Pollut* 145:219–224
36. Xu X, Sun Y, Fan Z, Zhao D, Xiong S, Zhang B, Liu G (2018) Mechanisms for ·O₂-and ·OH production on flowerlike BiVO₄ photocatalysis based on electron spin resonance. *Front Chem* 6:64
37. Uğurlu M, Gürses A, Doğar Ç, Yalçın M (2008) The removal of lignin and phenol from paper mill effluents by electrocoagulation. *J Environ Manag* 87:420–428
38. Bayat A, Shokri A (2021) Degradation of p-Nitrotoluene in aqueous environment by Fe (II)/Peroxy monosulfate using full factorial experimental design. *Sep Sci Technol* 56(17):2941–2950
39. Vaizoğullar Aİ, Uğurlu M, Ayyıldız A, Yılmaz Sİ, Chaudhary AJ (2017) TiO₂, WO₃, and V₂O₅, supported onactivated carbon: preparation, structural and catalytic behaviour in photocatalytic treatment of phenol and lignin from olive mill wastewater. *Fresenius Environmental Bulletin* 26(5):3529–3541
40. Shokri A (2022) Photocatalytic degradation of nitrotoluene in synthetic wastewater by CoFe₂O₄/SiO₂/TiO₂ nanoparticles using Box–Behnken experimental design. *Desalination Water Treat* 247:92–99
41. Xu R, Su M, Liu Y, Chen Z, Ji C, Yang M, Chen D (2020) Comparative study on the removal of different-type organic pollutants on hierarchical tetragonal bismutite microspheres: adsorption, degradation and mechanism. *J Clean Prod* 242:118366
42. Padmanaban VC, Giri Nandagopal MS, Madhangi Priyadarshini G, Maheswari N, Janani Sree G, Selvaraju N (2016) Advanced approach for degradation of recalcitrant by nanophotocatalysis using nanocomposites and their future perspectives. *Int J Environ Sci Technol* 13(6):1591–1606
43. Guan YH, Ma J, Li XC, Fang JY, Chen LW (2011) Influence of pH on the formation of sulfate and hydroxyl radicals in the UV/peroxy monosulfate system. *Environ Sci Technol* 45(21):9308–9314
44. Sun J, Li X, Zhao Q, Ke J, Zhang D (2014) Novel V₂O₅/BiVO₄/TiO₂ nanocomposites with high visible-light-induced photocatalytic activity for the degradation of toluene. *J Phys Chem C* 118:10113–10121
45. Karaoğlu MH, Uğurlu M (2010) Studies on UV/NaOCl/TiO₂/Sep photocatalysed degradation of Reactive Red 195. *J Hazard Mater* 174(2):864–871
46. Shokri A, Mahanpoor K (2018) Using UV/ZnO process for degradation of Acid red 283 in synthetic wastewater. *Bulgarian Chem Commun* 50(1):27–32
47. Badawy MI, Gohary FE, Ghaly MY, Ali MEM (2009) Enhancement of olive mill wastewater biodegradation by homogeneous and heterogeneous photocatalytic oxidation. *J Hazard Mater* 169(1-3):673–679
48. Galloni MG, Ferrara E, Falletta E, Bianchi CL (2022) Olive mill wastewater remediation: from conventional approaches to photocatalytic processes by easily recoverable materials. *Catalysts* 12(8):923
49. Akpan UG, Hameed BH (2009) Parameters affecting the photocatalytic degradation of dyes using TiO₂-based photocatalysts: A review. *J Hazard Mater* 170(2-3):520–529
50. Iboukhoulef H, Douani R, Amrane A, Chaouchi A, Elias A (2019) Heterogeneous Fenton like degradation of olive Mill wastewater using ozone in the presence of BiFeO₃ photocatalyst. *J Photochemistry Photobiol A: Chem* 383:112012
51. Justino CI, Duarte K, Loureiro F, Pereira R, Antunes SC, Marques SM, Freitas AC (2009) Toxicity and organic content characterization of olive oil mill wastewater undergoing a sequential treatment with fungi and photo-Fenton oxidation. *J Hazard Mater* 172(2-3):1560–1572
52. Iboukhoulef H, Amrane A, Kadi H (2016) Removal of phenolic compounds from olive mill wastewater by a Fenton-like system H₂O₂/Cu (II)—thermodynamic and kinetic modeling. *Desalination Water Treat* 57(4):1874–1879
53. Kallel M, Belaid C, Mechichi T, Ksibi M, Elleuch B (2009) Removal of organic load and phenolic compounds from olive mill wastewater by Fenton oxidation with zero-valent iron. *Chem Eng J* 150(2-3):391–395
54. Adhoum N, Monser L (2004) Decolourization and removal of phenolic compounds from olive mill wastewater by electrocoagulation. *Chem Eng Process: Process Intensif* 43(10):1281–1287
55. Lucas MS, Peres JA (2009) Removal of COD from olive mill wastewater by Fenton's reagent: Kinetic study. *J Hazard Mater* 168(2-3):1253–1259
56. Shokri A, Rabiee F, Mahanpoor K (2017) Employing a novel nanocatalyst (Mn/Iranian hematite) for oxidation of SO₂ pollutant in aqueous environment. *Int J Environ Sci Technol* 14:2485–2494

57. El Hajjoui H, Barje F, Pinelli E, Bailly JR, Richard C, Winterton P, Hafidi M (2008) Photochemical UV/TiO₂ treatment of olive mill wastewater (OMW). *Bioresour Technol* 99(15):7264–7269
58. Al-Malah K, Azzam MO, Abu-Lail NI (2000) Olive mills effluent (OME) wastewater post-treatment using activated clay. *Sep Purif Technol* 20(2-3):225–234
59. Al-Bsoul A, Al-Shannag M, Tawalbeh M, Al-Taani AA, Lafi WK, Al-Othman A, Alsheyab M (2020) Optimal conditions for olive mill wastewater treatment using ultrasound and advanced oxidation processes. *Sci Total Environ* 700:134576
60. Martins RC, Ferreira AM, Gando-Ferreira LM, Quinta-Ferreira RM (2015) Ozonation and ultrafiltration for the treatment of olive mill wastewaters: effect of key operating conditions and integration schemes. *Environ Sci Pollut Res* 22:15587–15597
61. Kirmaci A, Duyar A, Akgul V, Akman D, Cirik K (2018) Optimization of combined ozone/Fenton process on olive mill wastewater treatment. *Aksaray Univ J Sci Eng* 2(1):52–62
62. Domingues E, Fernandes E, Gomes J, Castro-Silva S, Martins RC (2021) Olive oil extraction industry wastewater treatment by coagulation and Fenton's process. *J Water Process Eng* 39:101818
63. Solís RR, Rivas FJ, Martínez-Piernas A, Agüera A (2016) Ozonation, photocatalysis and photocatalytic ozonation of diuron. *Intermed Identif; Chem Eng J* 292:72–81